*European Journal of Neuroscience, Vol. 15, pp. 1499–1508, 2002* 

# Epileptic fast activity can be explained by a model of impaired GABAergic dendritic inhibition

F. Wendling,[1] F. Bartolomei,[2] J. J. Bellanger[1] and P. Chauvel[2]
[1]Laboratoire Traitement du Signal et de L'Image, INSERM, Université de Rennes 1, Campus de Beaulieu, 35042 Rennes Cedex, France
[2]Laboratoire de Neurophysiologie et Neuropsychologie, INSERM, Université de la Méditerranée, 13385 Marseille Cedex 5, France

## Abstract

This paper focuses on high-frequency (gamma band) EEG activity, the most characteristic electrophysiological pattern in focal seizures of human epilepsy. It starts with recent hypotheses about: (i) the behaviour of inhibitory interneurons in hippocampal or neocortical networks in the generation of gamma frequency oscillations; (ii) the nonuniform alteration of GABAergic inhibition in experimental epilepsy (reduced dendritic inhibition and increased somatic inhibition); and (iii) the possible depression of $GABA_{A,fast}$ circuit activity by $GABA_{A,slow}$ inhibitory postsynaptic currents. In particular, these hypotheses are introduced in a new computational macroscopic model of EEG activity that includes a physiologically relevant fast inhibitory feedback loop. Results show that strikingly realistic activity is produced by the model when compared to real EEG signals recorded with intracerebral electrodes. They show that, in the model, the transition from interictal to fast ictal activity is explained by the impairment of dendritic inhibition.

*Keywords*: dis-inhibition, gamma band activity, interneuronal circuits, intracerebral EEG

## Introduction

High-frequency EEG waves originating from one or several brain regions are the most characteristic electrophysiological pattern in focal seizures of human epilepsy. Paradoxically, very few works are dedicated to their analysis compared to phasic interictal events. Low-voltage rapid discharges are often observed at seizure onset during presurgical evaluation of refractory partial epilepsies when intracerebral electrodes (depth-EEG) are used to record EEG signals. Low-amplitude waves with maximum frequencies belonging to the gamma band (20–100 Hz and beyond) (Bragin *et al*., 1999) have been reported in clinical studies (Allen *et al*., 1992). The regions they originate from are generally considered to be highly epileptogenic, and anatomically define a particular zone, referred to as the 'epileptogenic zone' Understanding of the epileptogenic zone network organization can lead to limited surgical resection aimed at suppressing seizures. Although fast EEG waves can now be well characterized from a signal-processing standpoint, underlying cellular mechanisms still remain to be understood. Here, potential clinical benefits are obvious: the understanding of neurophysiological and neurobiological factors implied in the generation of ictal fast waves could lead to the development of new therapeutic procedures aimed at neutralizing epileptogenic networks responsible for the initiation of seizures.

Modelling may be a way to progress in this understanding. Recently, studies based on experimental and/or computational models provided new insight in the understanding of neuronal mechanisms involved in rapid EEG activity.

On the one hand, there was evidence that oscillations of gamma frequency are linked to the behaviour of inhibitory interneurons in hippocampal or neocortical networks ('inhibition-based rhythms') (Jefferys *et al*., 1996; Whittington *et al*., 2000). On the other hand, results showed that two types of $GABA_A$ inhibitory postsynaptic currents (IPSCs) may play a crucial role in the formation of nested theta/gamma rhythms in hippocampal pyramidal cells (White *et al*., 2000).

In the field of epilepsy, the role of inhibition and the relationship between the inhibition/excitation balance and epileptogenesis have been largely investigated in experimental studies (Dichter, 1997). New advances now demonstrate that GABAergic inhibition that controls neuronal excitability is not uniformly altered in experimental temporal lobe epilepsy models; if dendritic inhibition is reduced, somatic inhibition is, in contrast, increased as a result of the hyperactivity of somatic projecting interneurons (Cossart *et al*., 2001).

In order to relate the aforementioned recent results to rapid activity (gamma band) observed in EEG seizure signals, we started from an existing macroscopic neurophysiologically relevant model of the EEG (neuronal population model) that differs from detailed microscopic models of interconnected individual neurons (Traub *et al*., 1997). The concepts upon which this model is based were initially developed by Freeman 1978) in their works dealing with perceptual processing in the olfactory system and, in the same time, by Lopes da Silva *et al*., (1974, 1976) in their study of the underlying mechanisms of alpha rhythm generation. In a previous study (Wendling *et al*., 2000), we showed that population models may explain several

*Correspondence*: Dr F. Wendling, as above.
Email: fabrice.wendling@univ-rennes1.fr

*Received 18 October 2001, revised 27 February 2002, accepted 15 March 2002*

doi:10.1046/j.1460-9568.2002.01985.x

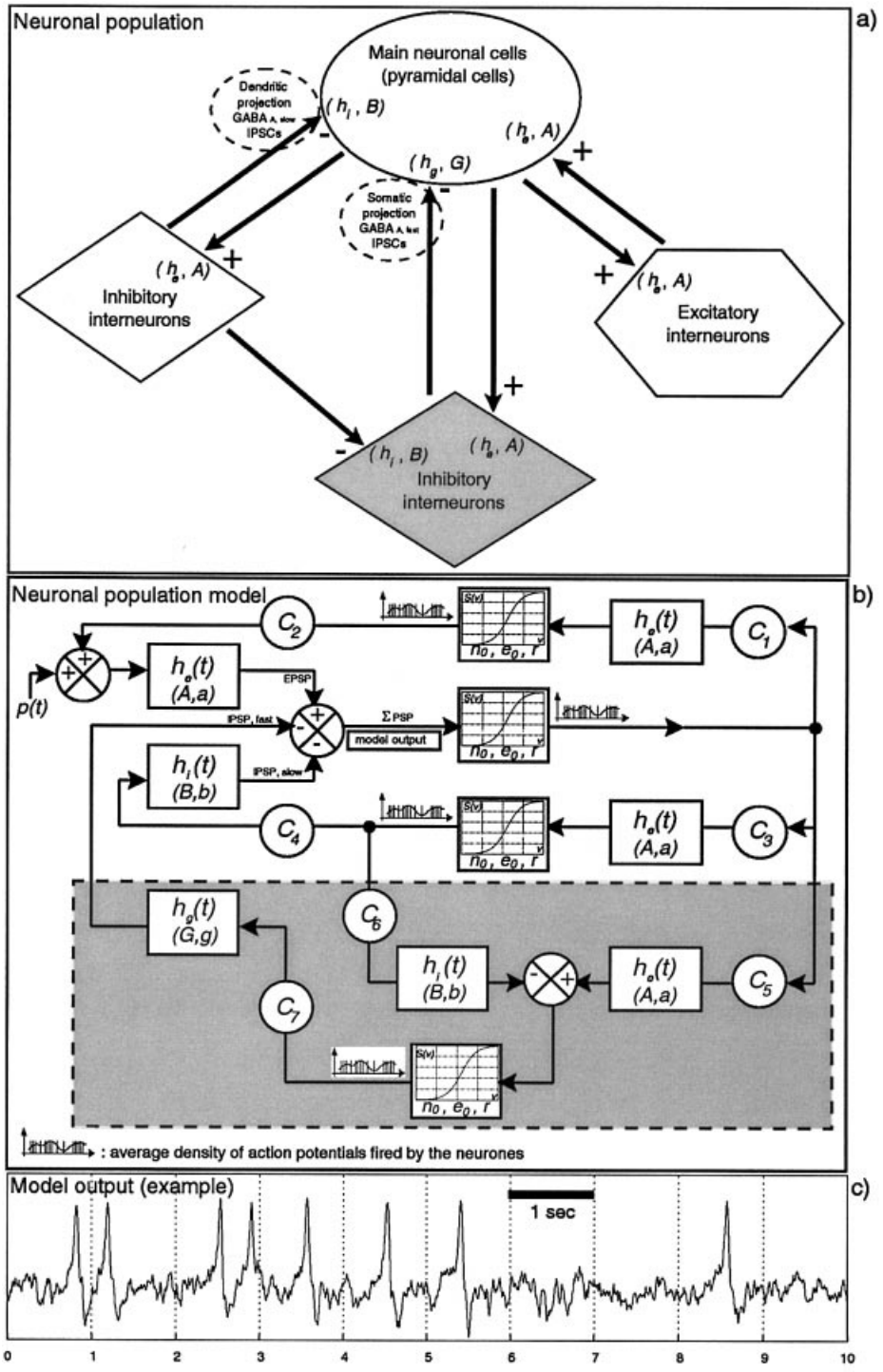


FIG. 1. From the hippocampal neuronal population organization to the neuronal population model. (a) Structurally, the neuronal population is considered to be composed of four neuronal subsets: pyramidal cells, excitatory interneurons, dendritic-projecting interneurons with slow synaptic kinetics ($GABA_{A,slow}$) and somatic-projecting interneurons (grey rectangle) with faster synaptic kinetics ($GABA_{A,fast}$). Subset of pyramidal cells project to and receive feedback from subsets of interneurons. As described in (Banks *et al*., 2000), dendritic interneurons project to somatic ones. (b) The model accounts for the neuronal population organization. In each subset, the average pulse density of afferent action potentials is changed into an average inhibitory or excitatory postsynaptic membrane potential using a linear dynamic transfer function of impulse response $h_e(t)$, $h_i(t)$, or $h_g(t)$, while this potential is converted into an average pulse density of potentials fired by the neurons using a static nonlinear function [asymmetric sigmoid curve, $S(v)$]. The subset of somatic-projecting interneurons (grey rectangle) receive input from both subsets of pyramidal and dendritic interneurons. (c) the model output represents the summated average postsynaptic potentials on pyramidal cells. It reflects an EEG signal.

rhythms observed in depth-EEG epileptic signals. Particularly, we demonstrated that realistic epileptiform activity can be simulated when model parameters are altered according to current hypotheses about epileptogenesis (balance between excitation and inhibition, excitatory couplings between distant neural populations). However, we also noticed that fast EEG activity cannot be produced when only a slow dendritic inhibitory loop is represented in the model. In the present article, we report an extension of the model that now takes into account recent hypotheses about: (i) the respective role of dendritic-projecting and somatic-projecting interneurons and (ii) the possible inhibition-related functional reorganizations that take place in the epileptic tissue.

The model is described in the next section and explored in the methods in terms of its three main parameters, namely dendritic excitation, dendritic inhibition and somatic inhibition provided by interneurons to pyramidal cells. Necessary conditions to obtain transitions between typical periods of epileptic activity, including low-voltage rapid discharges, are established. Under these conditions, very realistic signals are produced by the model. They are compared with real epileptic signals recorded *in vivo* in the human brain

Bartolomei *et al*., 2000 using intracerebral multiple lead electrodes (stereoelectroencephalography or SEEG, a diagnostic procedure used in the presurgical evaluation of patients suffering from refractory partial epilepsy). The results are then discussed with a special emphasis on the possible impairment of dendritic inhibition in the transition between interictal to ictal activity, as predicted by the model.

## The model

Different modelling strategies have been proposed to relate macroscopic EEG phenomena with oscillations in neuronal populations. In the paper of Whittington *et al*. (2000), two complementary approaches are presented. In the first one, referred to as 'detailed', single neurons are accurately modelled for their structural components (dendrites, soma and axon) and functional properties (voltage-dependent channels with kinetics derived from experimental voltage-clamp studies). Then, networks are built from the interconnection of a large enough number (i.e. several thousands) of neurons and different types of interneurons. In these networks, the EEG activity that corresponds to summated postsynaptic potentials that can develop on different parts of pyramidal cell membranes can be spatially and temporally studied for various parameters such as the types of neurons introduced in the network, network size, connectivity patterns or conduction delays. In the second one, referred to as 'reduced', a small number of neurons is used to better understand a particular dynamic behaviour, such as synchronization in networks of interneurons (White *et al*., 1998).

Besides these modelling techniques lying at the cellular and network levels, another approach lying at a higher level of organization, i.e. the population level, was proposed in the early 70 s. It starts from the fact that neurons form populations and that the EEG is a reflection of ensemble dynamics arising from interconnected populations of pyramidal cells and interneurons. This approach was initially proposed by Freeman (1978) and coworkers who made substantial progress in the understanding of perceptual processing in the olfactory system. Their studies, spanning the three last decades, are based on experimental data and on computational models in which the dynamics of each neural ensemble are represented by a 2nd order ordinary differential equation having a static nonlinearity identified as a asymmetric sigmoid curve (Eeckman & Freeman, 1991). They led to a model of the olfactory area able to produce EEG signals that approximate experimentally recorded EEGs quite accurately. Similar ideas developed at the same time by Lopes Da Silva *et al*. (1974) led to the development of a lumped-parameter population model able to explain the alpha rhythm of the EEG (Stam *et al*., 1999).

The EEG model upon which we have used follows the same approach but in a different context, namely the physiological interpretation of EEG signals recorded with intracerebral electrodes in epileptic patients according to the stereoelectroencephalographic method (Talairach & Bancaud, 1973).

In its earlier form, the model represented a cluster of neurons containing three interacting subsets. The first subset was composed of the main cells (i.e. pyramidal cells in the hippocampus or neocortex). It received a feedback from two other subsets composed of local interneurons, either excitatory or inhibitory. Model parameters were altered according to current hypotheses about epileptogenesis. Specifically, the influence of the balance between excitatory and inhibitory synaptic gains was analysed and conditions for realistic epileptiform activity, such as sustained discharges of spikes – a typical ictal pattern, to occur were found. It was also observed that the model was not able to represent fast EEG activity such as low-voltage rapid discharges often observed in depth-EEG signals at seizure onset. This fact was easily explained by the values of average synaptic time constants used in transfer functions of feedback loops in the model that act as low-pass filters and which are not compatible with experimentally observed frequencies (20–80 Hz).

In this new model version, a fourth subset is added in order to represent a second class of inhibitory interneurons with faster kinetics than those already included. This modification is based on bibliographical material. In the hippocampus, a series of studies based on a variety of techniques (Miles *et al*., 1996) demonstrate that there are two types of $GABA_A$ synaptic responses in CA1 pyramidal neurons: a fast one near the soma and a slow one in the dendrites. The first one ($GABA_{A,fast}$) is a rapidly activated and decaying IPSC mediated by somatic synapses and the second one ($GABA_{A,slow}$) is a slowly rising and decaying IPSC mediated by dendritic synapses. More recent works (White *et al*., 2000) suggest that two separate classes of interneurons (for simplicity called '$GABA_{A,fast}$ interneurons' and '$GABA_{A,slow}$ interneurons' in the following) give rise to these two IPSCs and show that the class of $GABA_{A,fast}$ interneurons mainly contribute to hippocampal gamma rhythms. Moreover, as suggested by Banks *et al*. (2000), both classes interact; $GABA_{A,slow}$ cells inhibit not only pyramidal cells but also $GABA_{A,fast}$ interneurons.

The model was re-designed in order to represent this functional organization of interacting subsets of principal cells and interneurons; it is summarized in Fig. 1a.

First, we added a new inhibitory feedback loop to the previous model in order to represent a subset of interneurons providing somatic inhibition to pyramidal cells ($GABA_{A,fast}$ interneurons). Like the two other classes of interneurons (excitatory and slow inhibitory), these interneurons receive excitatory input from pyramidal cells. However, they also receive afferent inhibitory input from $GABA_{A,slow}$ interneurons.

As, shown in Fig. 1b, the model consists of four subsets of neurons, namely the main cells (i.e. pyramidal cells), the excitatory interneurons, the slow dendritic-projecting inhibitory interneurons and the fast somatic-projecting inhibitory interneurons. The influence from neighbouring areas is represented by an excitatory input $p(t)$ (modelled by Gaussian white noise) that globally describes the average density of afferent action potentials. The model output corresponds to the postsynaptic activity of the first subset (summated postsynaptic potentials in activated pyramidal cells). It is interpreted as an EEG signal (Fig. 1c).

Each subset is characterized by: (i) a 2nd order linear transfer function that transforms the average presynaptic pulse density of afferent action potentials (the input) into an average postsynaptic membrane potential (the output), either excitatory, slow inhibitory or fast inhibitory with respective impulse response $h_e(t)$, $h_i(t)$ or $h_g(t)$, and (ii) a static nonlinear function – an asymmetric sigmoid function $S(v) = 2e_0/[1 + e^{r(v_0 - v)}]$ – that relates the average postsynaptic potential of a given subset to an average pulse density of potentials fired by the neurons.

Interactions between main cells and interneurons are summarized in the model by seven connectivity constants $C_1$ to $C_7$ which account for the average number of synaptic contacts.

Excitatory, slow inhibitory and fast inhibitory average postsynaptic membrane potentials are obtained from impulse responses given by $h_e(t) = A\ a.e^{-at}$, $h_i(t) = B\ b.e^{-bt}$ and $h_g(t) = G\ g.e^{-gt}$, respectively, with $t \geqslant 0$, where $A$, $B$ and $G$ represent the synaptic gains. They are shown in Fig. 2. Model parameter values are given in Table 1. The inhibitory feedback loop from the subset of fast somatic-projecting

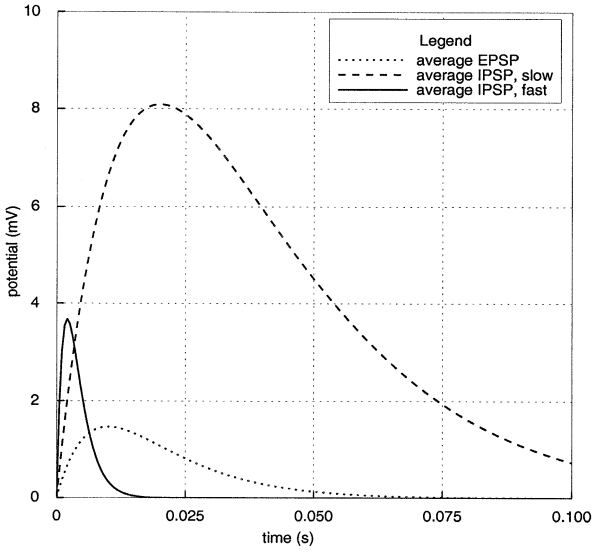


FIG. 2. Average postsynaptic membrane potentials: excitatory, slow inhibitory and fast inhibitory, respectively, obtained from impulse responses given by $h_e(t) = A\ a.e^{-at}$, $h_i(t) = B\ b.e^{-bt}$ and $h_g(t) = G\ g.e^{-gt}$, $t \geqslant 0$ (see Table 1 for parameter values).

inhibitory interneurons uses a faster impulse response $h_g(t)$ (i.e. producing faster IPSP) than $h_i(t)$. Here, the key parameter is the average somatic time delay $1/g$ which is chosen 10 times lower than the average dendritic time constant $1/b$, to be consistent with data provided in the book of Traub *et al.* (1999).

Starting from the fact that each linear transfer function $h_e(t)$, $h_i(t)$ and $h_g(t)$ introduces a pair of first order ordinary differential equations of the form:

$$\dot{z}_1(t) = z_2(t) \text{ and}$$

$$\dot{z}_2(t) = Wgx(t) - 2wz_2(t) - w^2z_1(t),$$

where $W = A$, $W = B$ or $W = G$ and $w = a$, $w = b$ or $w = g$, depending on the excitatory, slow inhibitory or fast inhibitory case, and where $x(t)$ and $z_1(t)$ are the respective input and output signals of the linear transfert functions, the following set of 10 differential equations that govern the population model can be easily established:

$$\dot{y}_0(t) = y_5(t)$$

$$\dot{y}_5(t) = AaS[y_1(t) - y_2(t) - y_3(t)] - 2ay_5(t) - a^2y_0(t)$$

$$\dot{y}_1(t) = y_6(t)$$

$$\dot{y}_6(t) = Aa\{p(t) - C_2S[C_1y_0(t)]\} - 2ay_6(t) - a^2y_1(t)$$

$$\dot{y}_2(t) = y_7(t)$$

$$\dot{y}_7(t) = BbC_4S[C_3y_0(t)] - 2by_7(t) - b^2y_2(t)$$

$$\dot{y}_3(t) = y_8(t)$$

$$\dot{y}_8(t) = GgC_7S[C_5y_0(t) - C_6y_4(t)] - 2gy_8(t) - g^2y_3(t)$$

$$\dot{y}_4(t) = y_9(t)$$

$$\dot{y}_9(t) = BbS[C_3y_0(t)] - 2by_9(t) - b^2y_4(t).$$

This set of equations is solved by classical numerical integration methods (Runge-Kutta, for example; Press *et al.*, 1993).

## Methods

As already mentioned, the model output represents an EEG signal. Six different types of EEG activity (numbered from 1 to 6, for simplicity) are produced by the model. They are shown in Fig. 3. From visual inspection, one can notice that they closely resemble real depth-EEG activity recorded interictally or ictally. Type 1 and type 2, respectively, refer to normal background activity and sporadic spikes as observed in real signals during interictal periods. Type 3 and type 4, respectively, refer to sustained spikes activity and slow rhythmic activity. Both may be encountered at seizure onset or during seizures. Type 5 refers to low-amplitude rapid discharges usually appearing at the beginning of ictal periods. Finally, type 6 refers to slow quasi-sinusoidal activity. It resembles real ictal activity that often follows rapid ictal activity in time.

These different types of activity depend on the three main parameter of the model, namely $A$, $B$ and $G$ that, respectively, correspond to excitatory, slow inhibitory and fast inhibitory synaptic gains in feedback loops from interneurons to pyramidal cells and in the control of fast inhibitory interneurons by slow ones. Therefore, we studied the model for these three parameters using a systematic procedure. In particular, for different values of $A$ (excitation), the ($B$, $G$) plane (slow inhibition, fast inhibition) was explored by varying $B$ and $G$ around standard values (see Table 1). A procedure allowing the type of activity produced by the model to be automatically recognized for each point in the ($B$, $G$) plane was elaborated. It is based on spectral features of simulated signals that are specific to each class of activity. Then, in order to globally represent the model behaviour as a function of $A$, $B$ *and* $G$, a coloured diagram, referred to as an 'activity map' was elaborated. This map corresponds to the ($B$, $G$) plane exploration performed for a given value of $A$ and in which a specific colour is used to encode the type of activity (from 1 to 6). This type is returned by the recognition procedure that automatically associates the signal simulated with a ($B$, $G$) value to one of the 6 possible classes of activity (Fig. 3a). Because $A$ was varied from 3 to 7 with a resolution of 0.5 mV, $B$ was varied from 0 to 50 mV with a resolution of 1 mV and $G$ was varied from 0 to 30 mV with a resolution of 1 mV, about 13500 simulations were performed. Each simulation produces an EEG segment of 20 s sampled at 200 Hz obtained by numerically integrating the set of equations presented in section 2.

As far as the Gaussian input noise is concerned, mean and variance were adjusted to obtain a rate ranging from 30 to 150 pulses per second, for which the model produces a signal similar to the normal background activity when other parameters are set to standard values (Table 1).

Finally, simulated periods of epileptic activity, as well as simulated transitions between them, are compared with real depth-EEG signals recorded in human hippocampus using intracerebral electrodes. Recordings were performed on a 128 channel BMSI acquisition system (Nicolet-BMSI, Madison, Wisconsin, USA). Signals are sampled at 200 Hz on a bandpass ranging from 0.16 Hz to 100 Hz.

## Results

Figure 4 shows activity maps obtained for different values of $A$ (excitation). Before analysing results in detail, general comments can be made from visual inspection of these maps. First, one may notice that regions in the ($B$, $G$) plane corresponding to the different types of activity produced by the model are relatively homogenous. Second, the region in red colour corresponding to rapid activity (type 5) starts to appear for increased values of $A$ (excitation) when values of $B$

TABLE 1. Model parameters, interpretation and values used to produce EEG signals

| Parameter | Interpretation | Standard value* |
|---|---|---|
| $A$ | Average excitatory synaptic gain | 3.25 mV |
| $B$ | Average slow inhibitory synaptic gain | 22 mV |
| $G$ | Average fast inhibitory synaptic gain | 10 mV |
| $1/a$ | Dendritic average time constant in the feedback excitatory loop | $a = 100\ s^{-1}$ |
| $1/b$ | Dendritic average time constant in the slow feedback inhibitory loop | $b = 50\ s^{-1}$ |
| $1/g$ | Somatic average time constant in the fast feedback inhibitory loop | $g = 500\ s^{-1}$ |
| $C_1$, $C_2$ | Average number of synaptic contacts in the excitatory feedback loop | $C_1 = C$, $C_2 = 0.8\ C$ (with $C = 135$) |
| $C_3$, $C_4$ | Average number of synaptic contacts in the slow feedback inhibitory loop | $C_3 = C_4 = 0.25\ C$ |
| $C_5$, $C_6$ | Average number of synaptic contacts in the fast feedback inhibitory loop | $C_5 = 0.3\ C$, $C_6 = 0.1\ C$ |
| $C_7$ | Average number of synaptic contacts between slow and fast inhibitory interneurons | $C_7 = 0.8\ C$ |
| $v_0$, $e_0$, $r$ | Parameters of the nonlinear asymetric sigmoid function (transforming the average membrane potential into an average density of action potentials) | $v_0 = 6$ mV $e_0 = 2.5\ s^{-1}$ r $= 0.56\ mV^{-1}$ |

*Standard values were established in Jansen & Rit (1995).

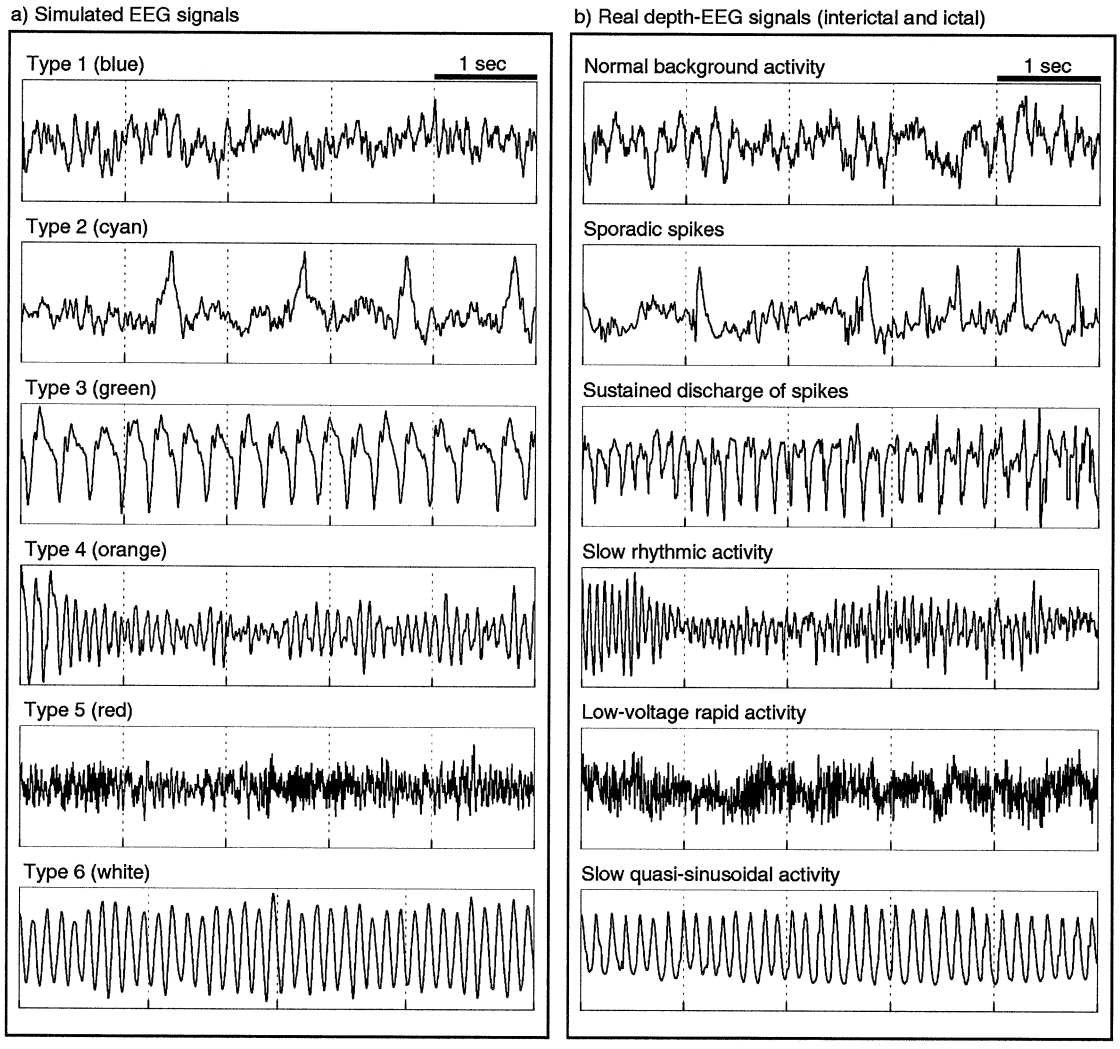


FIG. 3. (a) The different types of activity produced by the model and comparison with (b) real depth-EEG signals recorded in human hippocampus (during SEEG exploration and using intracerebral multiple lead depth-electrodes). In activity maps of Fig. 4, each type of activity is coded by the colour indicated in brackets.

(slow dendritic inhibition) decrease and values of $G$ (fast dendritic inhibition) stay constant. Third, slow quasi-sinusoidal activity (type 6) represented by the white region in the ($B$, $G$) plane appears for lower values of $G$. Finally, one can also see that the surface of the

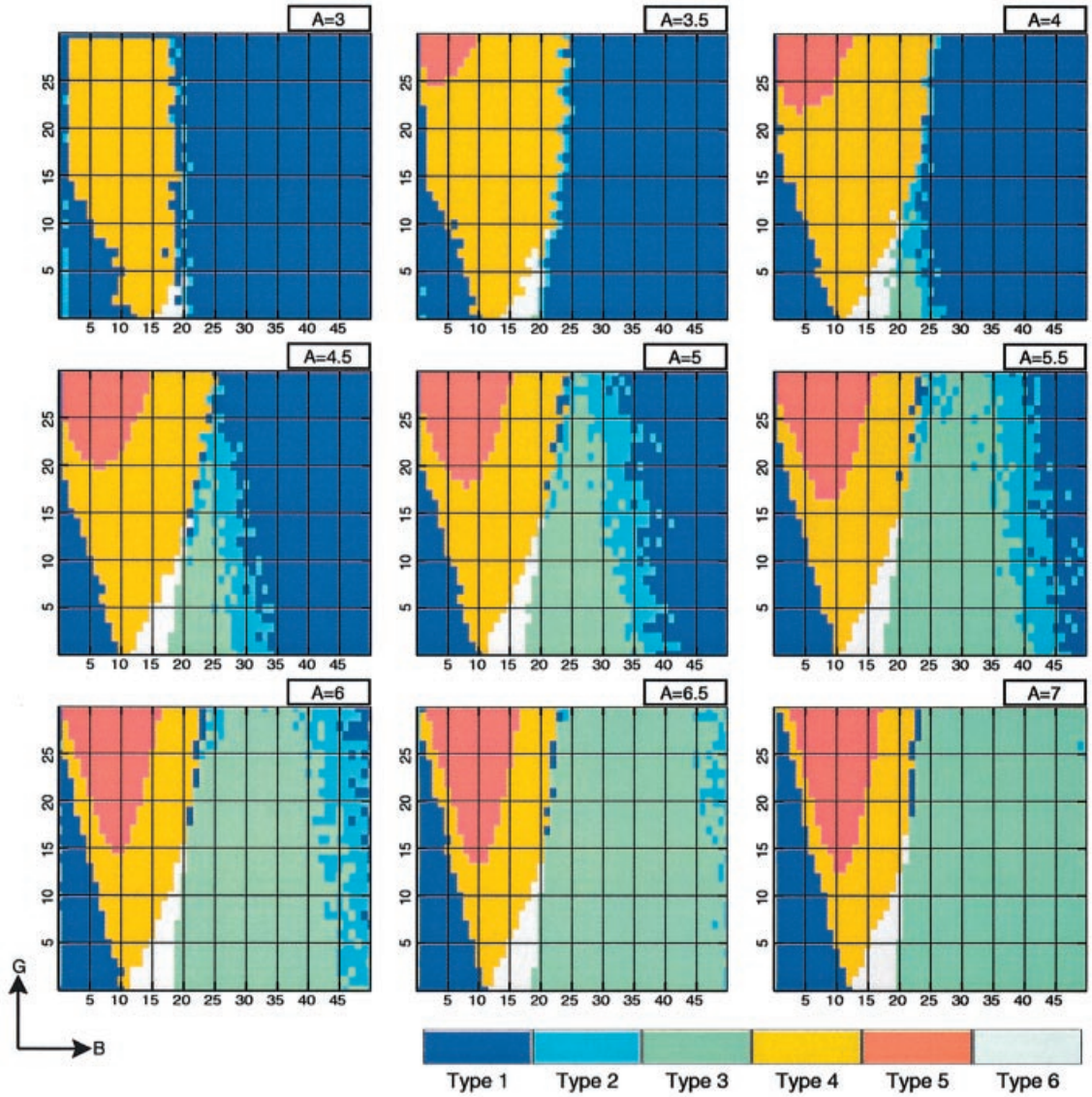


FIG. 4. Activity maps obtained for model exploration with respect to excitatory (*A*), slow inhibitory (*B*) and fast inhibitory (*G*) synaptic gains in feedback loops from interneurons to pyramidal cells.

green region (sustained spikes) increases with increased excitation, whereas the external contour of the orange region (slow rhythmic activity) stays almost constant with respect to *A*.

A more detailed analysis of activity maps reveals that for lower values of *A* (excitation) the main transition predicted by the model is that going from normal background activity (type 1) to slow rhythmic activity (type 4), respectively, represented by blue and orange regions. This type of transition is often encountered during ictal periods in real depth-EEG signals recorded from structures that do not generally belong to the epileptogenic zone. For these lower values of A (up to 4 mV), one can also observe that the surface of the red region corresponding to rapid activity is relatively small. For higher values of *A* (higher than 4 mV), two other types of activity start to appear: sporadic spikes (type 2) and sustained discharge of spikes (type 3), respectively, represented by cyan and green regions. Like rapid discharges (type 5), these two types of activity are also encountered in depth-EEG seizure signals. They are usually observed in epileptogenic structures. One may also underline that relevant transitions in signal dynamics are predicted by the model when dendritic dis-inhibition becomes effective: a transition from normal activity (blue region) to spiking activity (cyan and green regions), to slow rhythmic activity (orange region) and a transition to rapid discharges (red region).

The knowledge of activity maps generated from the model may be used to explain temporal dynamics of real electrophysiological signals observed during seizures. A first example is given in Fig. 5 which shows a real depth-EEG signal recorded in human hippocampus at the beginning of a partial temporal lobe epilepsy. Four phases (a-1 to a-4) are distinguished according to the pseudo-stationary nature of the activity reflected by the signal: normal background activity (type 1, phase a-1), discharge of rhythmic spikes (type 3, phase a-2), low voltage rapid discharge (type 5, phase a-3) and high-amplitude quasi-sinusoidal slower activity (type 6, phase a-4). The normalized power spectral density (PSD) shows that part of the rapid activity observed during phase a-3 belongs to the gamma band (55–60 Hz). It also shows that the frequency band corresponding to phase

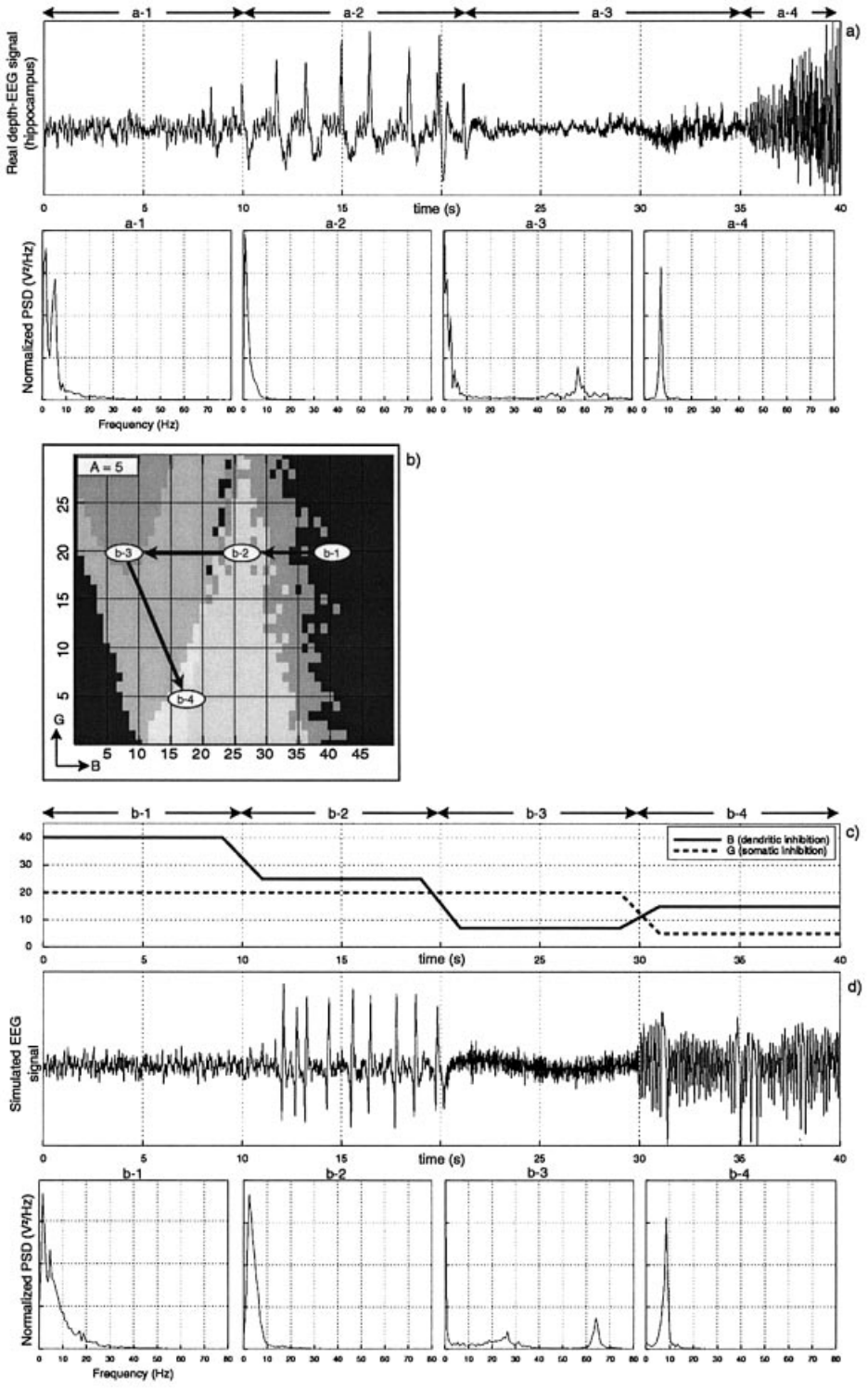


FIG. 5. (a) A real depth-EEG signal recorded in human hippocampus at the beginning of a partial temporal lobe seizure with intracerebral electrodes (SEEG). Four phases (a-1 to a-4) are distinguished according to the pseudo-stationary nature of the activity reflected by the signal: normal background activity (a-1), discharge of rhythmic spikes (a-2), low voltage rapid discharge (a-3) and high-amplitude quasi-sinusoidal slowing down activity (a-4). The normalized power spectral density (PSD) shows that part of the activity corresponding to phase a-3 belongs to the gamma band (55–60 Hz). (b) A candidate path on the activity map explaining the transitions of activity observed in the real signal (type 1 → type 3 → type 4 → type 6). (c) Slow and fast inhibitory synaptic gain profiles defined by the candidate path and used in the model to simulate a time-series signal with transitions in dynamics. (d) Simulated EEG signal obtained with the model when the synaptic gains vary as a function of time and PSDs computed on the four periods of 10 s (b-1 to b-4).

a-4 is extremely narrow (8–9 Hz), phenomenon often observed after rapid discharges. The observed sequence of transitions between periods of epileptic activity (type 1 → type 3 → type 4 → type 6) corresponds to a set of possible paths on the activity map, in the model. All these paths are orientated from right to left along the B axis, denoting a reduction of dendritic inhibition. In order to simulate time-series signals which temporal dynamics reproduce those observed in the real depth-EEG signal, we chose a candidate path (b-1 → b-2 → b-3 → b-4), shown in Fig. 5b, and characterized 4 steps: the initial step (b-1), corresponding to a standard (*B*, *G*) value, is followed by two consecutive reductions of dendritic inhibition (b-1 → b-2 and b-2 → b-3) with constant somatic inhibition and by further increase of dendritic inhibition (b-3 → b-4) with decreased somatic inhibition. From this path, and using an arbitrary value of 10 s per step, a temporal evolution of slow dendritic and fast somatic inhibitory gains *B* and *G*, shown in Fig. 5c, is obtained. These gain

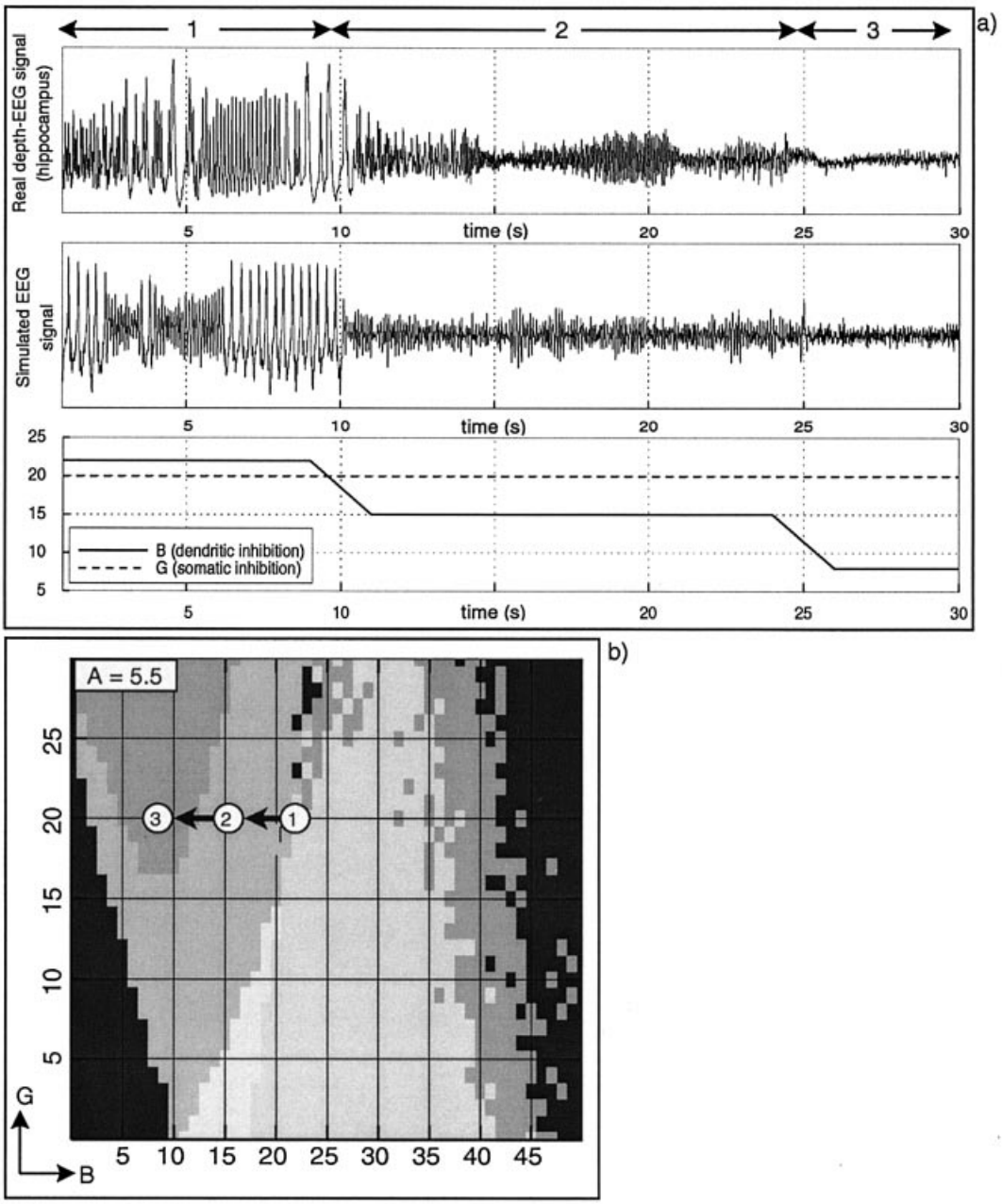


FIG. 6. (a) Another example of real depth-EEG signal recorded in human hippocampus at the beginning of a partial seizure along with the signal produced by the model using (b) a candidate path on the activity map ($1 \rightarrow 2 \rightarrow 3$). As in the previous example, changes in signal dynamics are explained, in the model, by a decrease in dendritic inhibition (*B*).

profiles are then used in the model to produce the time-series signal shown in Fig. 5d. As expected, the first decrease of the slow inhibition level leads the model to generate a sustained discharge of spikes (phase b-2), similar to that observed during the interictal to ictal activity in the real epileptic signal (phase a-2). The second decrease that allows fast inhibition to become active leads the model to generate a low-voltage rapid (gamma band) discharge (phase b-3) similar to that observed at seizure onset (phase a-3). Finally, the slower quasi-sinusoidal activity (phase b-4) is observed when fast inhibition weakens and slow inhibition increases. A similar type of activity often follows low-voltage rapid oscillations in real seizure signals (phase a-4). Finally, two comments may be made on this simulation example. First, transitions between periods of epileptic activity appear more abrupt than those observed in real signals. This is explained by the fact that parameters are abruptly changed from phase to phase during the simulation. Second, normalized PSD's corresponding to each 10 s portion show that characteristic frequencies present in simulated signals are close to those measured on pseudo-stationary periods of real signals.

A second simulation example is given in Fig. 6. As previously, the real depth-EEG signal (Fig. 6a) was recorded from the hippocampus at the beginning of a partial temporal lobe epilepsy in an epileptic patient undergoing presurgical evaluation. In this example, signals at seizure onset are characterized by a mixing of rhythmic spikes and

slow rhythmic activity. Then spikes disappear, and the slow rhythmic activity lasts for 10–15 s before a low-amplitude rapid discharge is observed. Using the same qualitative identification procedure, we may define a path characterized by 3 steps on the activity map: a 10-s initial phase (1) for which the activity is at the frontier between sustained spikes (green region) and slow rhythmic activity (orange region) followed by 15-s phase (2, orange region) of slow rhythmic activity, followed itself by a 5-s rapid discharge (3, red region). Here, inhibitory gain profiles simply correspond to a dendritic dis-inhibition while somatic inhibition stays constant. From these profiles, the time-series signal shown in the second panel of Fig. 6a is produced by the model. As in the previous example, one may notice that this signal is quite realistic although precise waveform fit is not the primary intent of the simulation.

## Discussion and conclusion

In a previous study (Wendling *et al*., 2000), we emphasized the potential interest of nonlinear lumped parameter models in the analysis of depth-EEG epileptic signals. Starting from the concept of neuronal population model initially proposed by Lopes Da Silva *et al*. (1974) and Freeman (1978), we developed a model of coupled neuronal populations able to produce realistic mutichannel epileptiform EEG signals. However, a model shortcoming was the impossibility of producing rapid activity.

In the present study, recently published hypotheses about: (i) the behaviour of inhibitory interneurons in the generation of gamma frequency oscillations; (ii) the impairment of dendritic GABAergic inhibition in experimental epilepsy; and (iii) the depression of $GABA_{A,fast}$ circuit activity by $GABA_{A,slow}$ inhibitory postsynaptic currents have been introduced in a new model of hippocampal neuronal population belonging to the same class of macroscopic neurophysiological models. This model includes two main features: a fast inhibitory feedback loop that represents somatic projections from the subset of $GABA_{A,fast}$ interneurons onto the subset of pyramidal cells and an inhibitory control on the former subset by the subset of dendritic $GABA_{A,slow}$ interneurons, as suggested in by Banks *et al*. (2000).

These modifications allowed the model to generate rapid EEG oscillations in addition to other types of activity. Results obtained from visual inspection and from estimation of power spectral densities show that simulated epileptiform activity is realistic even if precise curve fitting is not the aim of simulations. The different types of activity generated by the model depend on three main parameters: excitatory, slow inhibitory and fast inhibitory synaptic gains in feedback loops from interneurons to pyramidal cells and in the control of fast inhibitory interneurons by slow ones. When the model is explored with respect to these three parameters, results show that it may predict relevant transitions between the different types of activity, either from the interictal to the ictal period or during the ictal period itself. These transitions are explained, in the model, by the increase of excitability (imbalance between excitatory and inhibitory processes). Precisely, transition to ictal epileptiform activity is explained by the impairment of slow dendritic inhibition (or 'dis-inhibition'). From a pathophysiological standpoint, these results suggest that mechanisms involved in low-voltage rapid discharges (a characteristic pattern observed at seizure onset in human partial epilepsy) may be directly linked to inhibitory processes: a reduction of GABAergic dendritic inhibition would allow somatic inhibitory interneurons to abnormally and continuously generate fast IPSP's on pyramidal cells.

As suggested in (Cossart *et al*., 2001), this impairment of GABAergic dendritic inhibition in the epileptic tissue could be explained by a selective loss of inhibitory interneurons projecting to stratum lacunosum moleculare and controlling the excitability of pyramidal neuron's dendrites. This impairment (reproduced, in the model, by the reduction of parameter $B$, i.e. the average slow inhibitory synpatic gain) could first lead, at the EEG level, to a rhythmic discharge of spikes or to a slow rhythmic activity (appearing with the increase of the excitation : inhibition ratio), followed by the low-voltage rapid discharge when the dis-inhibition of fast inhibitory interneurons is sufficiently marked. These findings are in agreement with results described by Penttonen *et al*. (1998) suggesting that rapid discharges reflect rhythmic postsynaptic potentials in hyperpolarized pyramidal cells brought about by rhythmically discharging somatic-projecting interneurons. Finally, from a computational modelling standpoint, these results demonstrate that the macroscopic level of the model (neural population) is well suited to the macroscopic nature of real depth-EEG signals (recorded with intracerebral macroelectrodes). They also suggest that this class of models which differs from that of more microscopic models can be adapted to a specific cerebral structure when data about architectonics and functional organization are available. Insights into neurophysiological mechanisms (related to the balance/imbalance between inhibitory and excitatory processes) underlying the generation of EEG epileptic signals may be expected from such models, especially when confronted to real data either obtained from clinical investigation of epileptic patients or from experimental studies.

## Acknowledgements

The authors wish to thank the two referees for their constructive suggestions and valuable comments on the present work.

## Abbreviations

PSD, power spectral density; SEEG, stereoelectroencephalography.

## References

Allen, P.J., Fish, D.R. & Smith, S.J. (1992) Very high-frequency rhythmic activity during SEEG suppression in frontal lobe epilepsy. *Electroencephalogr. Clin. Neurophysiol.*, **82**, 155–162.

Banks, M.I., White, J.A. & Pearce, R.A. (2000) Interactions between distinct GABA (A) circuits in hippocampus. *Neuron*, **25**, 449–457.

Bartolomei, F., Wendling, F., Bellanger, J.J., Chauvel, P. (2001) Neural networks involved in temporal lobe seizures: a nonlinear regression analysis of SEEG signals interdependencies. *Clin. Neurophysiol*., **112**, 1746–1760.

Bragin, A., Engel, J. Jr, Wilson, C.L., Fried, I. & Mathern, G.W. (1999) Hippocampal and entorhinal cortex high-frequency oscillations (100–500 Hz) in human epileptic brain and in kainic acid – treated rats with chronic seizures. *Epilepsia*, **40**, 127–137.

Cossart, R., Dinocourt, C., Hirsch, J.C., Merchan-Perez, A., De Felipe, J., Ben-Ari, Y., Esclapez, M. & Bernard, C. (2001) Dendritic but not somatic GABAergic inhibition is decreased in experimental epilepsy. *Nature Neurosci.*, **4**, 52–62.

Dichter, M.A. (1997) Basic mechanisms of epilepsy: targets for therapeutic intervention. *Epilepsia*, **38**, S2–S6.

Eeckman, F.H. & Freeman, W.J. (1991) Asymmetric sigmoid non-linearity in the rat olfactory system. *Brain Res.*, **557**, 13–21.

Freeman, W.J. (1978) Models of the dynamics of neural populations. *Electroencephalogr. Clin. Neurophysiol.*, **34**, 9–18.

Jansen, B.H. & Rit, V.G. (1995) Electroencephalogram and visual evoked potential generation in a mathematical model of coupled cortical columns. *Biol. Cybern.*, **73**, 357–366.

Jefferys, J.G., Traub, R.D. & Whittington, M.A. (1996) Neuronal networks for induced '40 Hz' rhythms. *Trends Neurosci.*, **19**, 202–208.

Lopes da Silva, F.H., van Rotterdam, A., Barts, P., van Heusden, E., Burr, W. (1976) Models of neuronal populations: The basic mechanisms of rhythmicity. *Prog. Brain Res*., **45**, 281–308.

Lopes da Silva, F.H., Hoeks, A., Smits, H. & Zetterberg, L.H. (1974) Model of brain rhythmic activity. The alpha-rhythm of the thalamus. *Kybernetik*, **15**, 27–37.

Miles, R., Toth, K., Gulyas, A.I., Hajos, N. & Freund, T.F. (1996) Differences between somatic and dendritic inhibition in the hippocampus. *Neuron*, **16**, 815–823.

Penttonen, M., Kamondi, A., Acsady, L. & Buzsaki, G. (1998) Gamma frequency oscillation in the hippocampus of the rat: intracellular analysis in vivo, *Eur. J. Neurosci.*, **10**, 718–728.

Press, W.H., Teukolsky, S.A., Vetterling, W.T. & Flannery, B.P. (1993) Integration of Ordinary Differential Equations. In *Numerical recipes in C: The art of scientific computing*. Cambridge University Press, Cambridge.

Stam, C.J., Pijn, J.P., Suffczynski, P. & Lopes da Silva, F.H. (1999) Dynamics of the human alpha rhythm: evidence for non-linearity? *Clin. Neurophysiol.*, **110**, 1801–1813.

Talairach, J. & Bancaud, J. (1973) Stereotaxic approach to epilepsy: methodology of anatomo-functional stereotaxic investigations. *Progr. Neurol. Surg.*, **5**, 297–354.

Traub, R.D., Jefferys, J.G.R. & Whittington, M.A. (1997) Simulation of gamma rhythms in networks of interneurons and pyramidal cells. *J. Comput. Neurosci*., **4**, 141–150.

Traub, R.D., Jefferys, J.G.R. & Whittington, M.A. (1999) *Fast Oscillations in Cortical Circuits.* MIT Press, Cambridge, MA; London.

Wendling, F., Bellanger, J.J., Bartolomei, F. & Chauvel, P. (2000) Relevance of nonlinear lumped-parameter models in the analysis of depth-EEG epileptic signals. *Biol. Cybern.*, **83**, 367–378.

White, J.A., Banks, M.I., Pearce, R.A. & Kopell, N.J. (2000) Networks of interneurons with fast and slow gamma-aminobutyric acid type A (GABAA) kinetics provide substrate for mixed gamma-theta rhythm. *Proc. Natl Acad. Sci. USA*, **97**, 8128–8133.

White, J., Chow, C., Ritt, J., Soto-Trevino, C. & Kopell, N. (1998) Synchronization and oscillatory dynamics in heterogeneous, mutually inhibited neurons,. *J. Comp. Neurosci.*, **5**, 5–16.

Whittington, M.A., Traub, R.D., Kopell, N., Ermentrout, B. & Buhl, E.H. (2000) Inhibition-based rhythms: experimental and mathematical observations on network dynamics,. *Int. J. Psychophysiol.*, **38**, 315–336.